

ENVIRONMENTAL RESEARCH LETTERS

LETTER • OPEN ACCESS

Estimating centennial-scale changes in global terrestrial near-surface wind speed based on CMIP6 GCMs

To cite this article: Cheng Shen *et al* 2021 *Environ. Res. Lett.* **16** 084039

View the [article online](#) for updates and enhancements.

ENVIRONMENTAL RESEARCH LETTERS**OPEN ACCESS****RECEIVED**
19 April 2021**REVISED**
28 June 2021**ACCEPTED FOR PUBLICATION**
12 July 2021**PUBLISHED**
30 July 2021

Original content from this work may be used under the terms of the Creative Commons Attribution 4.0 licence.

Any further distribution of this work must maintain attribution to the author(s) and the title of the work, journal citation and DOI.

**LETTER**

Estimating centennial-scale changes in global terrestrial near-surface wind speed based on CMIP6 GCMs

Cheng Shen¹ , Jinlin Zha^{2,3,*} , Deming Zhao² , Jian Wu³, Wenxuan Fan³ , Mengxi Yang⁴ and Zhibo Li⁵

¹ Gaochun Meteorological Bureau, Nanjing 211300, People's Republic of China

² CAS Key Laboratory of Regional Climate and Environment for Temperate East Asia, Institute of Atmospheric Physics, Chinese Academy of Sciences, Beijing 100029, People's Republic of China

³ Key Laboratory of Atmospheric Environment and Processes in the Boundary Layer over the Low-Latitude Plateau Region, Department of Atmospheric Science, Yunnan University, Kunming 650091, People's Republic of China

⁴ Taizhou Meteorological Observatory, Taizhou 225300, People's Republic of China

⁵ Laboratory for Climate and Atmosphere-Ocean Studies, Department of Atmospheric and Oceanic Sciences, School of Physics, Peking University, Beijing 100871, People's Republic of China

* Author to whom any correspondence should be addressed.

E-mail: zhajl@tea.ac.cn

Keywords: near-surface wind speed, CMIP6, centennial-scale changes, stilling, reversal

Supplementary material for this article is available [online](#)

Abstract

A global terrestrial stilling in recent decades has been reported, but the centennial-scale changes in global terrestrial near-surface wind speed (NSWS) and the potential contributing factors are yet to be revealed. Consequently, in this study, centennial-scale changes in global terrestrial NSWS are investigated based on Coupled Model Intercomparison Project phase 6 datasets, and that the potential factors causing those changes are detected. The results show that the global annual mean NSWS increased from 1850 to 1967 ($+0.0045 \text{ m s}^{-1} \text{ decade}^{-1}$, $p < 0.01$), with significant increases in North America, Europe, Africa, and South Asia. However, the NSWS decreased from 1968 to 2014 ($-0.0044 \text{ m s}^{-1} \text{ decade}^{-1}$, $p < 0.01$), significantly so in the mid-to-high latitudes of the Northern Hemisphere. The seasonal mean NSWS also increased before the 1960s and decreased thereafter. However, the NSWS over South America and most of Southern Africa increased during the study period. The changes in NSWS were caused mainly by changes in the number of strong windy days. The increase in NSWS from 1850 to 1967 could be attributed to internal variability, and the decrease in NSWS from 1968 to 2014 could be attributed to natural, aerosol, and greenhouse-gas forcings. However, internal variability acted mainly to increase the NSWS from 1968 to 2014, and so it is suggested that the contributions of external forcings to the global terrestrial stilling after the 1960s were considerable.

1. Introduction

Investigating changes in near-surface wind speed (NSWS) facilitates the understanding of atmospheric circulation, improves climate analysis and prediction. As more countries commit to emissions reductions by mid-century to curb anthropogenic climate change, decarbonization of the electricity sector becomes a first-order task in reaching this goal. Renewable, particularly wind power, will be predominant component of this transition (Sherman *et al* 2017, 2021). A rapid increase in wind power

capacity has been predicted in many countries and regions (Pryor *et al* 2020). The NSWS changes have a considerable influence on the wind energy resource (He *et al* 2010). NSWS also shows effects on global and regional evapotranspiration (Roderick *et al* 2007, Liu *et al* 2014), visibility (Sun *et al* 2018, Zhang *et al* 2020a), agriculture, and ecosystems (Deng *et al* 2021). The intensification of NSWS may exacerbate soil erosion, thereby generating more-severe dust storms (Alizadeh-Choobari *et al* 2014, Guan *et al* 2017, Segovia *et al* 2017, Zhang *et al* 2019a, 2020b). Consequently, investigating the long-term changes in

NSWS is beneficial to the assessment of wind energy and environmental and ecological issues related to NSWS.

Previous studies have reported long-term decrease in global NSWS (Vautard *et al* 2010, Zhang *et al* 2019b). The reduction in NSWS has also been observed at regional scale, including in China (Guo *et al* 2011, Lin *et al* 2013, Wu *et al* 2016, Zha *et al* 2017, 2021a), Australia (McVicar *et al* 2012), Czech Republic (Brazdil *et al* 2009), Switzerland (McVicar *et al* 2010), United Kingdom (Earl *et al* 2013), Turkey (Dadaser-Celik and Cengiz 2014), South Korea (Kim and Paik 2015), Spain and Portugal (Azorin-Molina *et al* 2014, 2016), and Brazil (Gilliland and Keim 2018). Roderick *et al* (2007) referred to these declining trends in NSWS as ‘stilling’. The long-term reduction in NSWS is also revealed by reanalyses, but which is weaker in reanalyses than that in observations (You *et al* 2010, Zhang and Wang 2020). Recent studies mainly analyzed the climatology, interannual variability, and trends of NSWS at global and regional scales (Torralba *et al* 2017, Ramon *et al* 2019, Wohland *et al* 2019), and the spatiotemporal characteristics of global NSWS at centennial scale are yet to be revealed.

Some studies also discovered a weak increase in NSWS over the past decade. Zeng *et al* (2019) referred to this phenomenon as ‘reversal’. The reversal of stilling has also been discovered at regional scale. For instance, the annual mean NSWS increased over South Korea after 2003 (Kim and Paik 2015), southwestern China after 2000 (Yang *et al* 2012), northwestern China after 1993 (Li *et al* 2018), and eastern China after 2010 (Zha *et al* 2021b). Zeng *et al* (2019) highlighted the major role of ocean–atmosphere oscillations in explaining stilling versus reversal. We proposed that stilling and reversal could be a cyclical, decadal pattern of NSWS at the centennial-scale (Shen *et al* 2021).

Compared to the investigation of historical NSWS, the projections of NSWS are investigated rarely at global scale. Based on the Coupled Model Intercomparison Project Phase 5 (CMIP5), the wind speed at the end of this century are projected to reduce in most regions of globe (Chen *et al* 2012, Kumar *et al* 2015). Karnauskas *et al* (2018) pointed out that the wind power reduction in future was located mainly in the mid-latitudes across the Northern Hemisphere (NH) and increase over the tropics and Southern Hemisphere (SH). Based on a multi-model ensemble of CMIP5, Sherman *et al* (2021) suggested that available wind resource over China and India will decline slightly. However, what are the main features of NSWS at centennial-scale during the historical period? The investigation of historical wind speed changes at centennial-scale could provide a scientific basis for the projections of wind speed.

The NSWS changes are influenced by internal variability and external forcings (Wu *et al* 2018a).

Internal variability affecting NSWS are attributed to the changes of large-scale ocean–atmosphere circulations. For instance, the NSWS changes over the NH could be influenced by the Tropical Northern Atlantic (TNA), the Pacific Decadal Oscillation (PDO), and the North Atlantic Oscillation (NAO) (Zeng *et al* 2019). El Niño/Southern Oscillation (ENSO) is a result of sea–air interaction on multiple space-time scales, which has a significant effect on the Asian monsoons and PDO (Ni *et al* 1995, Fu *et al* 2011, Lu *et al* 2016). We have revealed that the ENSO has a considerable effect on NSWS in China (Shen *et al* 2021). External forcings impact on NSWS is attributed to anthropogenic activities, including land use and cover change (Zha *et al* 2016, 2019, Zhang *et al* 2019b), anthropogenic aerosol emissions (Li *et al* 2016), and greenhouse gas (GHG) emissions (Jiang *et al* 2010, Zha *et al* 2020). Deng *et al* (2021) analyzed the global NSWS based on CMIP6 and suggested that the NSWS in NH decreased from 1980 to 2010, and that the attribution analysis was focused mainly on revealing the differences between land and ocean NSWSs. Unfortunately, the centennial-scale changes in terrestrial NSWS and the potential factors contributing to those changes were not investigated.

Consequently, the novelty of this study compared to previous ones is twofold: (a) spatiotemporal characteristics of the centennial-scale changes in global terrestrial NSWS are investigated based on CMIP6 models; (b) potential factors causing decadal changes in NSWS at centennial scale are detected. The results presented herein help to improve the understanding of global terrestrial NSWS changes.

2. Datasets and methods

2.1. Datasets

Multi-model simulations of NSWS from CMIP6 are used. The simulations are distinguished by their ‘rip’ index, which denotes the initial states (r), initialization methods (i), physics versions (p), and the forcing datasets (f) for CMIP6 (Grose *et al* 2020, Jian *et al* 2020, Parding *et al* 2020). This study uses the first ensemble member (‘r1i1p1f1’) each from a group of 33 models that were available at the time of writing (table S1). CMIP6 offers improved spatial resolution and physical parameterization compared to CMIP5 (Eyring *et al* 2016, 2019). To reveal the factors inducing centennial-scale variability in NSWS, the Detection and Attribution Model Intercomparison Project (DAMIP) is used. Only ten models of DAMIP were available at the time of writing (table S1). Based on DAMIP, four main forcings affecting NSWS changes are discussed: (a) aerosol forcing (anthropogenic-aerosol-only historical simulations (BC, OC, SO₂, SO₄, NO_x, NH₃, CO, NMVOC): hist-aer experiment in DAMIP), (b) GHG forcing (well-mixed GHG-only historical simulations: hist-GHG experiment in

DAMIP), (c) natural forcing (natural-only historical simulations (solar irradiance, stratospheric aerosol); hist-nat experiment in DAMIP), and (d) internal variability (Historical simulation experiment minus main external forcing experiment (hist-GHG, hist-aer, hist-CO₂)). It is worth noting that the internal variability is assuming linearity of the GHG, aerosol and natural variability responses. Details for DAMIP are given in Gillett *et al* (2016).

Four centennial-scale reanalyses with daily mean wind speed are used to compare with the CMIP6: (a) the European Centre for Medium-Range Weather Forecasts (ECMWF) 20th-century reanalysis assimilating surface observations only (ERA-20C) that is produced with ECMWF Integrated Forecasting System version Cy38r1 (Poli *et al* 2013), (b) the ECMWF ten-member ensemble of coupled climate reanalyses of the 20th century (CERA-20C) that is produced with Integrated Forecasting System version Cy41r2 (Hersbach *et al* 2015), (c) the National Oceanic and Atmospheric Administration (NOAA)-Cooperative Institute for Research in Environmental Sciences (CIRES) 20th-century reanalysis version 2 (NOAA-CIRES-20CR-V2C) that is produced by the Earth System Research Laboratory Physical Sciences Division from NOAA and the University of Colorado CIRES (Compo *et al* 2011), and (d) NOAA-CIRES-DOE 20th-century reanalysis version 3 (NOAA-CIRES-20CRV3) that is the new version of the 20th-century reanalysis (Slivinski *et al* 2019). Details for these reanalyses are presented in table S2.

2.2. Methods

A piecewise linear function (PWLF) is used to fit the trends of NSWS during different periods. PWLF automatically detect the optimal turning point (TP) and allowing multiple linear models to be fitted to each distinct section of the time series (Fyllas *et al* 2009, Jekel and Venter 2019). A PWLF can be described as follows

$$\gamma(t) = \begin{cases} \alpha_1 + \beta_1(t - b_1) & b_1 < t < b_2 \\ \alpha_2 + \beta_2(t - b_2) & b_2 < t < b_3 \\ \vdots & \\ \alpha_{n_b-1} + \beta_{n_b-1}(t - b_{n_b-1}) & b_{n_b-1} < t < b_{n_b} \end{cases}, \quad (1)$$

where b_1 is the location of the first breakpoint, b_2 is the location of the second breakpoint, and so forth until the last breakpoint b_{n_b} . $\alpha_1, \alpha_2, \dots, \alpha_{n_b-1}$ and $\beta_1, \beta_2, \dots, \beta_{n_b-1}$ are the regression coefficients. In cases where the TPs are unknown, global optimization is used to find the best set of TPs that minimizes the overall sum-of-square of the residuals (Storn and Price 1997). Multiple TPs can be set; however, in order to avoid overfitting, we assume that there is one and only one TP during the entire study period. The necessity of introducing the TP is examined with the

significance *t*-test under the null hypothesis that ' β is not different from zero'. If the maximum of the absolute value for β is occurred in a given year, that year is determined to be the TP. Statistical significance for the regression include the goodness-of-fit, the *P* value for the entire model, and the trends before and after the TP (Zha *et al* 2021b).

The variance of wind speed is calculated based on annual mean value of NSWS (equation (2))

$$V_x = \frac{1}{n} \sum_{i=1}^n (x_i - \bar{x})^2, \quad (2)$$

where V_x denote the variance of NSWS, n denote the total time period, x_i denote the NSWS, and \bar{x} denote the mean value of NSWS. We calculate the multi-model ensemble (MME) mean of NSWS firstly and then calculate the variance.

A Gaussian low-pass filter is used to determine the decadal signals of NSWS with a nine-year time window and an empirical orthogonal function (EOF) is used to partition the wind fields into a set of orthogonal modes consisting of spatial structures and corresponding time series (Wu *et al* 2017, 2018b, 2018c). All datasets are interpolated onto the $1.0^\circ \times 1.0^\circ$ resolution grid using bilinear interpolation. To evaluate the frequency trends for different categories of windy days, four windy days are defined based on their wind speed percentiles: (a) light windy days (<25th percentile), (b) gentle windy days (between 25th and 50th percentiles), (c) moderate windy days (between 50th and 75th percentiles), and (d) strong windy days (>75th percentile) (Zha *et al* 2021b). The trends of annual/seasonal NSWS and frequency trends for different categories of windy days are calculated based on the least-square method. We calculate the ensemble mean of multi-models for NSWS firstly and then calculate the trends and variances (Wu *et al* 2020). Four seasons are defined as boreal winter (December, January, and February (DJF)), spring (March, April, and May (MAM)), summer (June, July, and August (JJA)), and autumn (September, October, and November (SON)).

3. Results

3.1. Spatiotemporal characteristics of global NSWS at centennial scale

Temporal evolutions of NSWS in the MME mean at centennial scale are shown in figure 1. Annual mean NSWS increased from 1850 to 1967 ($+0.0045 \text{ m s}^{-1} \text{ decade}^{-1}$, $p < 0.01$) and decreased thereafter ($-0.0044 \text{ m s}^{-1} \text{ decade}^{-1}$, $p < 0.01$) (figure 1(a)). Seasonally, the NSWS also increased before 1967 and decreased after, with the strongest increase in winter ($+0.0060 \text{ m s}^{-1} \text{ decade}^{-1}$, $p < 0.01$) (figure 1(b)) and the strongest decrease in spring ($-0.0063 \text{ m s}^{-1} \text{ decade}^{-1}$, $p < 0.01$) (figure 1(c)). The TPs were inconsistent among

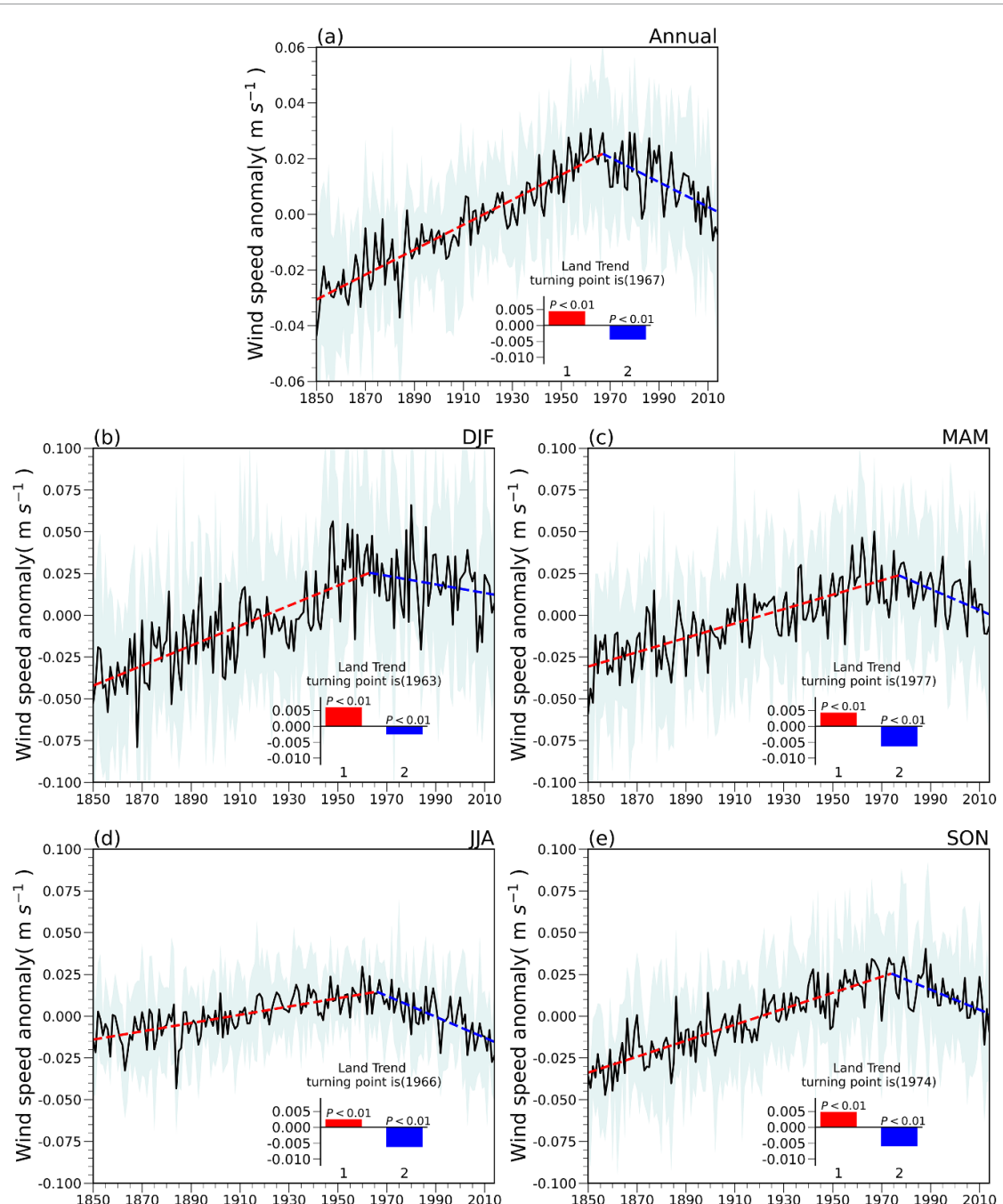


Figure 1. Temporal evolutions of (a) global annual mean near-surface wind speed (NSWS) anomaly and (b–e) seasonal mean NSWS anomaly from 1850 to 2014 in the multi-model ensemble (MME) mean of CMIP6 global climate models. The shading denotes the uncertainty spread determined by all CMIP6 models. The red and blue lines are the fitted lines based on the piecewise linear function (PWLF). The trends based on the PWLF are shown in the inset. $p < 0.01$ indicates that the goodness-of-fit of the PWLF passes the significance test at the 0.01 level. DJF: December, January, and February. MAM: March, April, and May. JJA: June, July, and August. SON: September, October, and November.

the seasons but mainly located in and around the 1960s. Previous studies have reported a decrease in global NSWS since 1960s (Vautard *et al* 2010, Zhang *et al* 2019b). The spatial patterns of trend changes among models were also compared (figures S1 and S2 (available online at stacks.iop.org/ERL/16/084039/mmedia)), and most models also mainly exhibited an increase in NSWS from 1850 to 1967 (figure S1) and a decrease in NSWS from 1968 to 2014 (figure S2). However, the differences of trends among models are considerable.

The EOF was used to assess whether the aforementioned centennial-scale changes were the pre-dominant signals in NSWS (figure S3). The spatial pattern of the first mode of the EOF mainly exhibited positive values across globe from 1850 to 1967, and the time series of the first mode exhibited an increase with the explained variance of 32.86%, which passed the significance *North* test (figures S3(a) and S3(b)). From 1968 to 2014, the spatial pattern of the first mode of the EOF mainly exhibited negative values over the mid-to-high latitudes of NH and

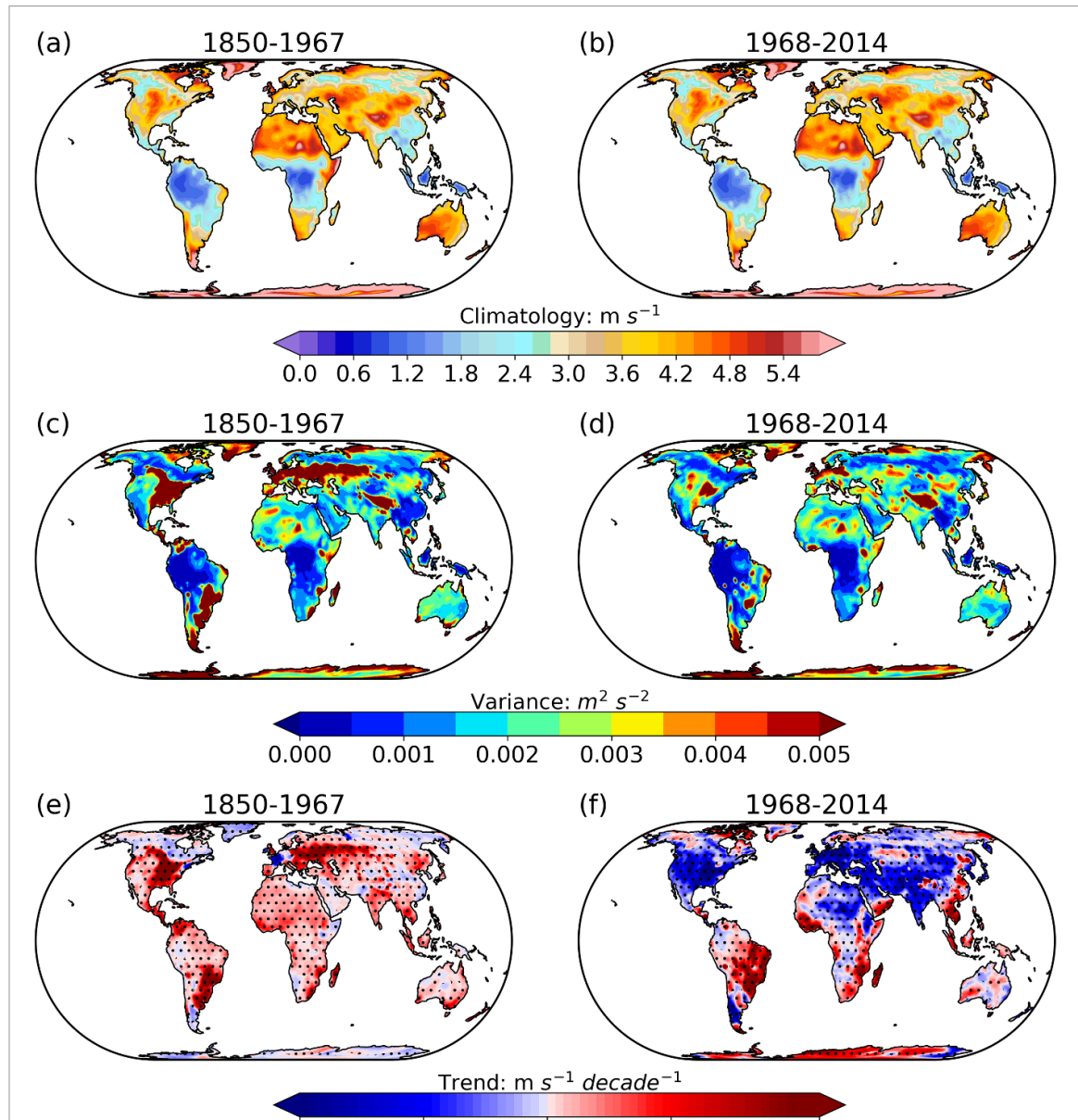


Figure 2. Spatial patterns of (a, b) mean NSWS, (c, d) NSWS variance, and (e, f) trends of NSWS during the two periods. The dots in (e) and (f) indicate that the trends pass the significance *t*-test at the 0.10 level.

positive values over SH; furthermore, the time series also exhibited an increase with the explained variance of 18.57%, which passed the significance *North* test (figures S3(c) and S3(d)). Consequently, the NSWS changes from increasing to decreasing should be the predominant signals in NSWS changes at centennial scale. To demonstrate whether the aforementioned characteristics of NSWS based on the CMIP6 models can be produced in global reanalysis products, NSWS changes in four analyses are also analyzed (figure S4). The NSWS showed a characteristic from increasing to decreasing in the selected four centennial-scale reanalyses, although the interannual variability, trends and TPs were inconsistent with those from CMIP6.

The mean values and variances of NSWS from 1850 to 1967 and from 1968 to 2014 displayed similar spatial pattern. There was no distinct difference

in NSWS climatology during the two periods. The large values of NSWS mainly located in North America, North Africa, Central Asia, and Australia, and the small values of NSWS mainly located in South America, Southern Africa, and East Asia (figures 2(a) and (b)). The large values of variance mainly located in eastern part of North America, Europe, and Central Asia (figures 2(c) and (d)), implied that the NSWS showed strong interannual and interdecadal changes in these regions. A significant difference was found in the NSWS trends during the two periods. The NSWS mainly increased from 1850 to 1967, with significant increases over North America, Europe, Africa, and South Asia (figure 2(e)). From 1968 to 2014, the NSWS decreased over the NH (e.g. in North America, Europe, Central Asia, and South Asia) and increased over the SH (e.g. in South America and Southern

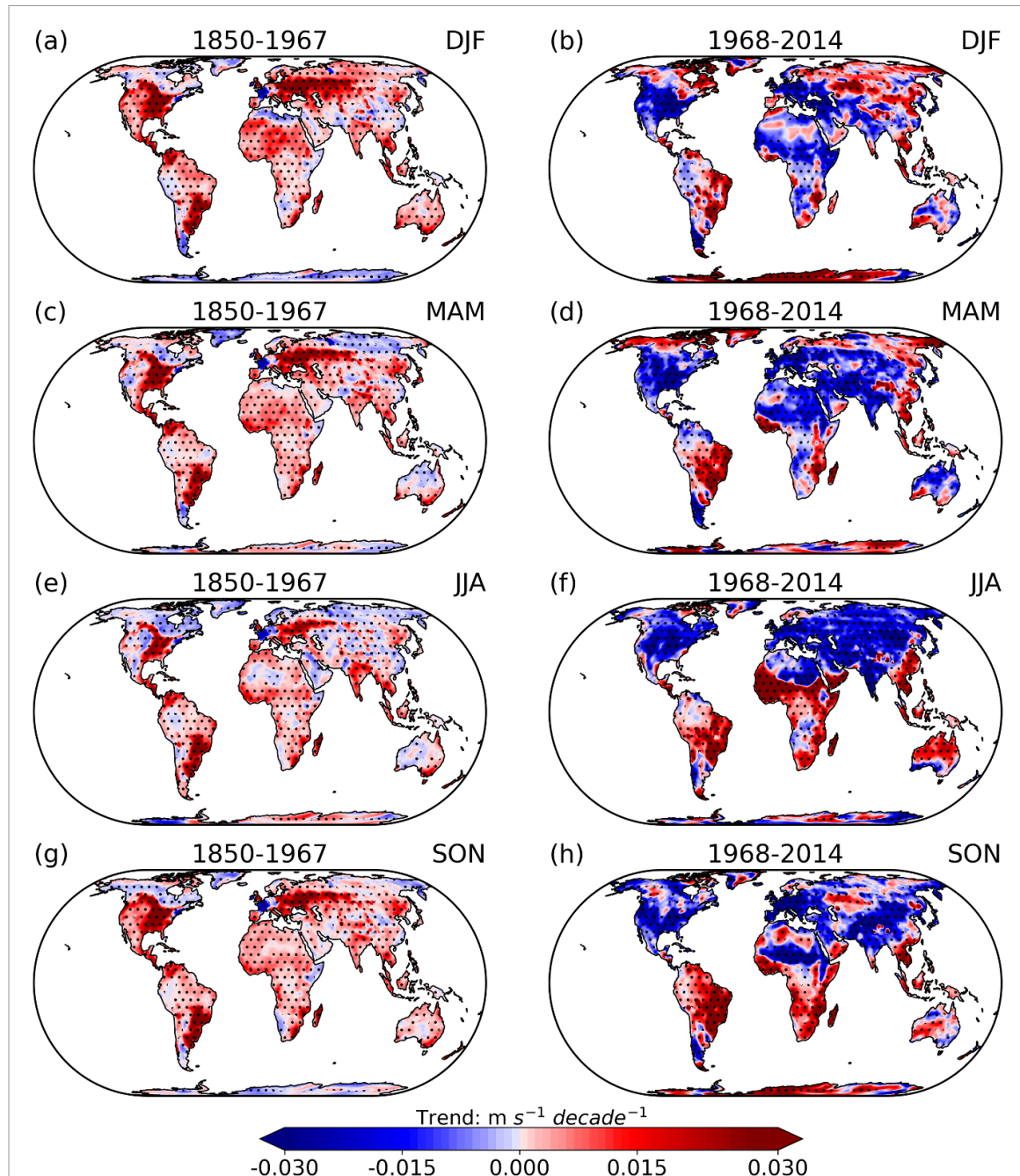


Figure 3. Spatial patterns of trends of seasonal mean NSWS during 1850–1967 and 1968–2014. The dots indicate that the trends pass the significance *t*-test at the 0.10 level. The four seasons are defined as the boreal winter (DJF) (a, b), spring (MAM) (c, d), summer (JJA) (e, f), and autumn (SON) (g, h).

Africa) (figure 2(f)). The significant differences of seasonal NSWS changes were also found in the trends (figure 3); however, the mean values and variances of seasonal NSWS showed similar spatial patterns during the two periods (figures S5 and S6). From 1850 to 1967, the global NSWS tended to increase in each season (figures 3(a), (c), (e) and (g)); however, it mainly decreased over the NH and increased over the SH from 1968 to 2014 (figures 3(b), (d), (f) and (h)). These characteristics were more significant in summer (figure 3(f)) and autumn (figure 3(h)) than other seasons.

Overall, the changes in global NSWS generated a transition since 1960s that occurred mainly at mid-to-high latitudes in the NH. In the SH, particularly in South America and Southern Africa, the NSWS has been increasing in all seasons. The global mean NSWS increased before 1960s and decreased after, which was the primary features of NSWS changes. However, the NSWS did not change uniformly throughout world. The global mean NSWS changes from increasing to decreasing at centennial scale did not mean that this characteristic presented everywhere. The NSWS changes showed regional difference.

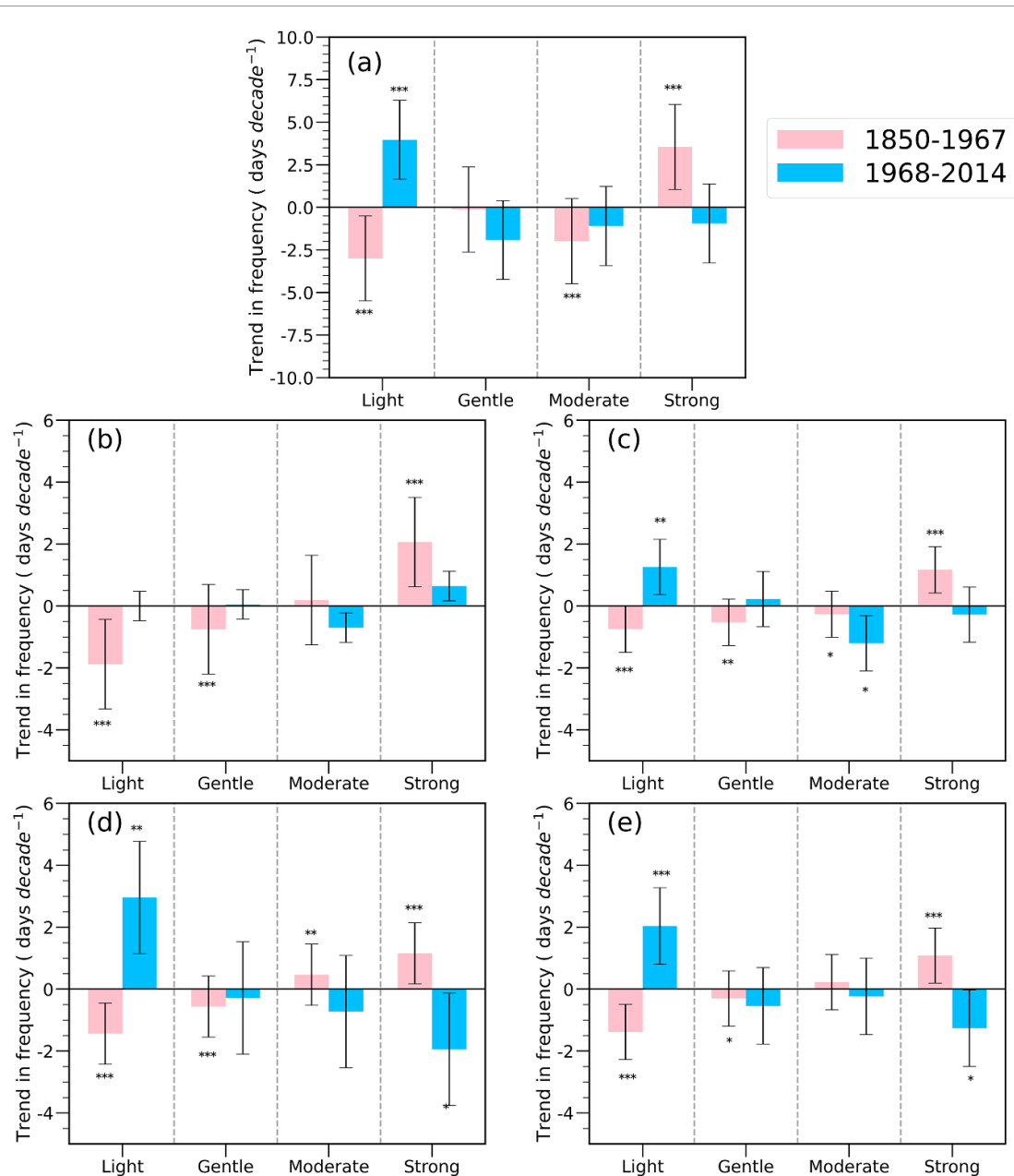


Figure 4. Linear trends of annual and seasonal frequencies of different wind categories (light, gentle, moderate, and strong) (unit: days decade $^{-1}$) for 1850–1967 and 1968–2014. (a)–(e) show annual mean, winter (DJF), spring (MAM), summer (JJA), and autumn (SON), respectively. Different windy days are defined as follows: light windy days (<25th percentile), gentle windy days (between 25th and 50th percentiles), moderate windy days (between 50th and 75th percentiles), and strong windy days (>75th percentile). *, **, and *** indicate that the trends pass the significance t-test at the 0.10, 0.01, and 0.001 levels, respectively. The black bars denote the uncertainties of the results.

3.2. Trends for different categories of windy days during the two periods at centennial scale

The decadal changes in NSWS at centennial scale could cause the changes in frequencies of different windy days, so the frequency trends for different windy days are investigated (figure 4). From 1850 to 1967, the number of strong windy days increased ($+3.54$ days decade $^{-1}$; $p < 0.001$), while the numbers of light and moderate windy days decreased, at the rates of -3.00 ($p < 0.001$) and -1.98 days decade $^{-1}$ ($p < 0.001$), respectively. The number of strong windy days also increased in all seasons from 1850 to 1967, with the strongest increase

in winter ($+2.06$ days decade $^{-1}$; $p < 0.001$) and the weakest increase in autumn ($+1.08$ days decade $^{-1}$; $p < 0.001$). Compared to figure 1, the significant increases in annual and seasonal mean NSWSS from 1850 to 1967 were due mainly to the increase in the number of strong windy days and decrease in the number of light windy days. From 1968 to 2014, the numbers of all categories of windy days decreased except for light windy days ($+3.97$ days decade $^{-1}$; $p < 0.001$) (figure 4(a)). Seasonally, the number of light windy days increased, with the most significant increase in summer ($+2.96$ days decade $^{-1}$; $p < 0.01$) (figure 4(d)). The numbers of moderate

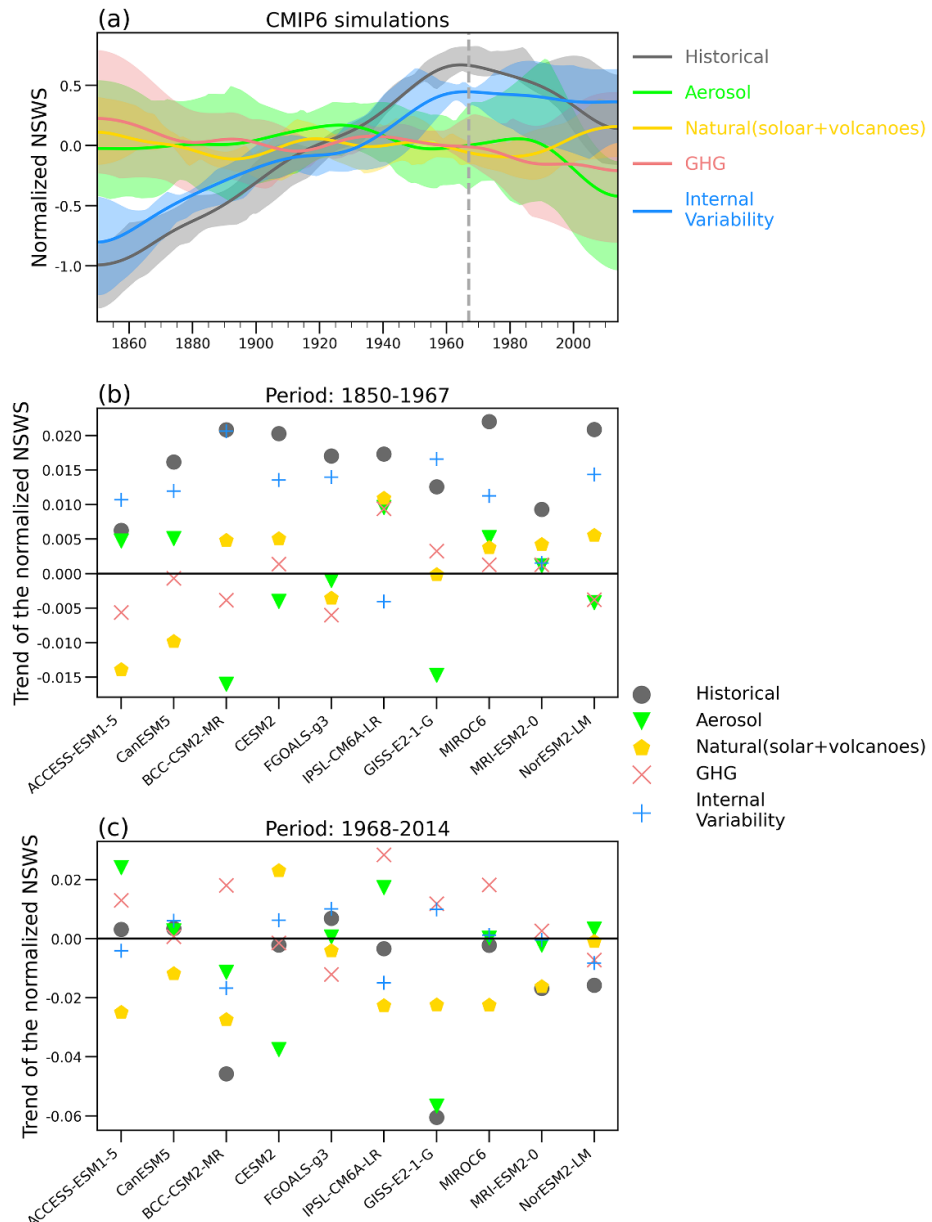


Figure 5. Temporal evolutions of normalized near-surface wind speed (NSWS) from 1850 to 2014 (a), and trends of normalized NSWS in single Detection and Attribution Model Intercomparison Project (DAMIP) model during (b) from 1850 to 1967 and (c) from 1968 to 2014. In (a), the shading denotes the uncertainty spread determined by all ten DAMIP models. In (b) and (c), the black lines denote the zero curves of trends. The trends are calculated using the normalized NSWS.

and strong windy days in all seasons decreased except for strong windy days in winter, with the most significant decreases in spring ($-1.20 \text{ days decade}^{-1}$; $p < 0.1$) for moderate windy days and summer ($-1.94 \text{ days decade}^{-1}$; $p < 0.1$) for strong windy days. Accordingly, the pronounced decrease in NSWSs from 1968 to 2014 were due mainly to the decreases in the numbers of strong and moderate windy days.

3.3. Potential factors causing centennial-scale changes in NSWS

The potential factors causing the centennial-scale changes in NSWS are detected based on the ten DAMIP models of CMIP6. Actually, these models can

also capture the characteristics of NSWS changes during the study period, i.e. increasing before 1960s and decreasing after (figure S7).

Temporal evolutions of NSWS in different forcings are shown in figure 5. In the experiment with internal variability, the NSWS increased significantly from 1850 to 1967, consistent with the historical NSWS changes. With aerosol and natural forcings, the NSWS neither increased nor decreased significantly from 1850 to 1967. With GHG forcing, the NSWS decreased during the period (figure 5(a)). However, with only aerosol forcing experiment, the NSWS decreased in the MME of DAMIP after the 1960s. The NSWS trends among different models from 1850 to 1967 and from 1968 to 2014 are also

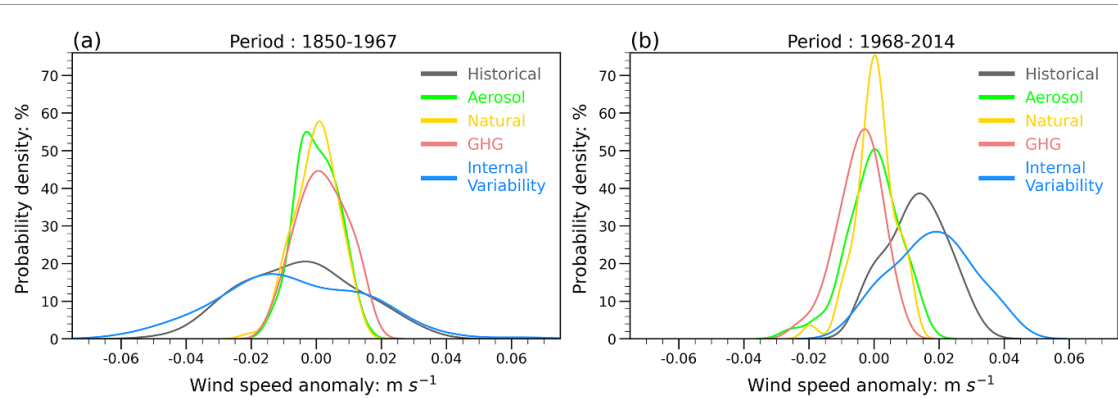


Figure 6. Probability density function (PDF) of near-surface wind speed (NSWS) under different forcings during (a) 1850–1967 and (b) 1968–2014. The PDFs of NSWSs are calculated based on the monthly mean values of wind speeds, and the anomaly of wind speed is calculated under different forcings in itself, respectively.

compared (figures 5(b) and (c)). The increase in historical NSWS from 1850 to 1967 was due mainly to internal variability, which was discovered in nine of the ten DAMIP models, and no other forcing gave rise to pronounced NSWS strengthening from 1850 to 1967 (figure 5(b)). However, from 1968 to 2014, the decrease in historical NSWS was due mainly to natural, aerosol, and GHG forcings; for aerosol forcing in particular, most of the DAMIP models displayed decreased NSWS (figure 5(c)).

How the different forcings affect the probability density function (PDF) of NSWS is investigated (figure 6). The PDF of NSWS anomalies with internal variability was closer to that of the historical NSWS during the two periods compared to the other forcings, but the PDF moved toward larger positive NSWS anomalies after the 1960s. Consequently, it was mainly internal variability that increased NSWS after the 1960s. During the two periods, the NSWS PDFs with aerosol, natural, and GHG forcings were higher and narrower than the historical NSWS PDF. From 1850 to 1967, the mean values of NSWS anomalies with aerosol, GHG, and natural forcings were close to zero, but not so with internal variability. By contrast, after the 1960s, the mean values of NSWS anomalies with aerosol and GHG forcings were negative, whereas the contributions of internal variability to NSWS changes were positive. Therefore, external forcings (aerosol and GHG forcings) decreased the NSWS after the 1960s.

Spatial patterns of NSWS trends under different forcings are also analyzed (figure 7). From 1850 to 1967, accompanied by GHG, natural, and aerosol forcings, the NSWS mainly decreased, strongly so in North America and Eurasia; however, the increase in NSWS from 1850 to 1967 was due mainly to internal variability (figure 7(g)). Compared to figure 2(e), the increase in global NSWS from 1850 to 1967 was due mainly to internal variability. From 1968 to 2014, the NSWS also mainly decreased accompanied by GHG, natural, and aerosol forcings, but the decrease in NSWS accompanied by these factors from 1968

to 2014 was more pronounced than that from 1850 to 1967. Note that the increase in NSWS from 1968 to 2014 was due mainly to internal variability, especially in East Asia, South America, and Africa. Therefore, the NSWS would decrease more significantly from 1968 to 2014 if the effects of internal variability were excluded. Compared figure 7 with figure 2(f), the reduction of NSWS in figure 7 was weaker than that in figure 2(f). Consequently, we proposed that the GHG, natural, and aerosol forcings could induce the NSWS reduction from 1968 to 2014; however, there was not any single factor that significantly dominate the reduction in NSWS. It is worth noting that aerosol and GHG affect the NSWS change at the centennial-scale could show uncertainty due to the internal variability cannot be well excluded based on the MME of CMIP6. Furthermore, the uncertainty of aerosol and GHG influence on NSWS may also be generated from the model bias (Bichet *et al* 2012, Deng *et al* 2021).

4. Conclusions and discussions

The centennial-scale variability in global terrestrial NSWS is discussed, and the potential factors causing centennial-scale changes in NSWS were revealed based on CMIP6 global climate models in this study. The main results are as follows.

- From 1850 to 1967, the global annual mean terrestrial NSWS increased, and the significant increases were found in North America, Europe, Africa, and South Asia. From 1968 to 2014, the global annual mean terrestrial NSWS decreased, and the significant decreases were found in North America, Europe, Central Asia, and South Asia. The mean values and variances of NSWS during the two periods showed similar spatial patterns, and therefore there was no distinct difference in NSWS climatology during the two periods. The significant difference of global terrestrial NSWS changes at the centennial scale was shown in the NSWS trends. Global annual

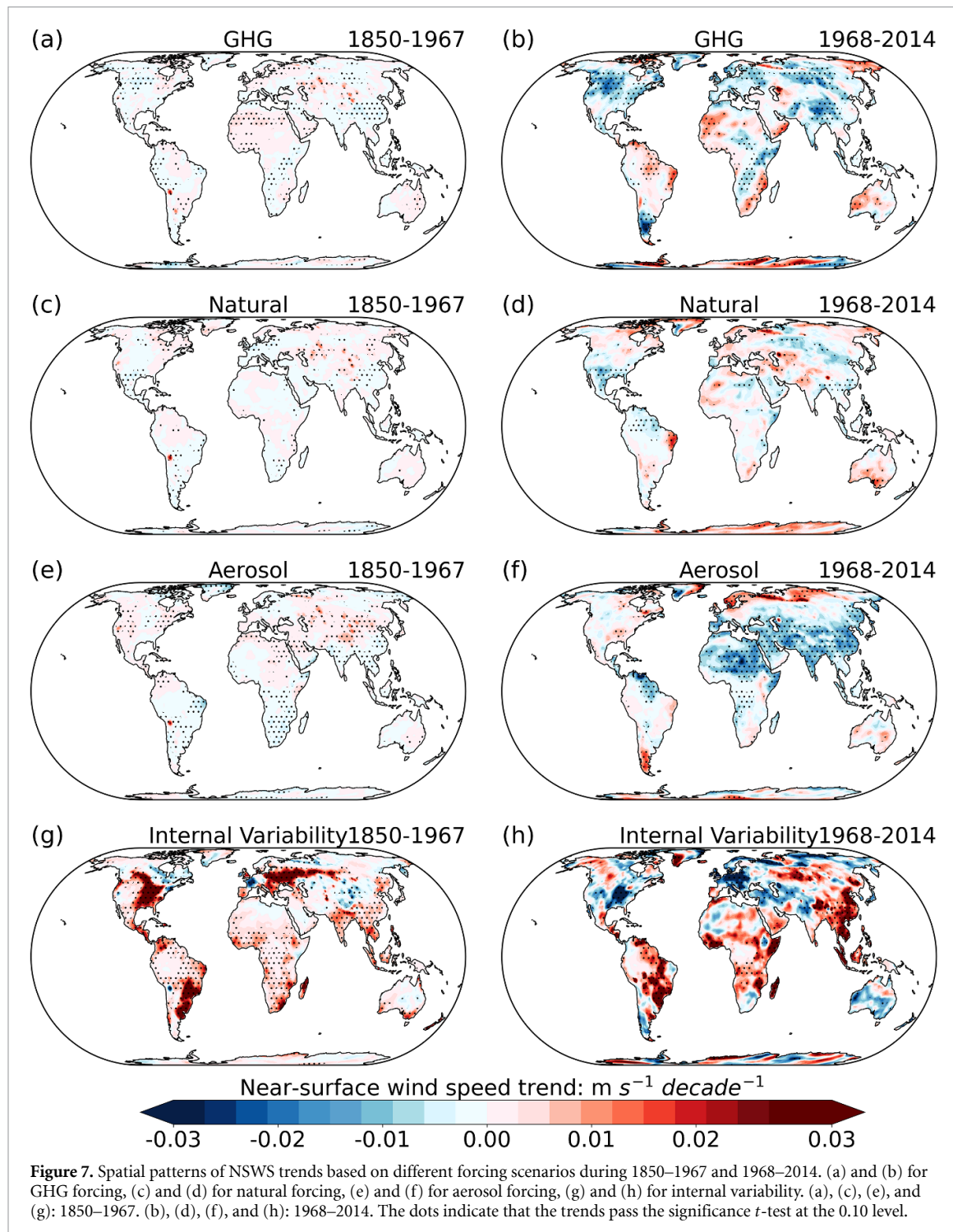


Figure 7. Spatial patterns of NSWS trends based on different forcing scenarios during 1850–1967 and 1968–2014. (a) and (b) for GHG forcing, (c) and (d) for natural forcing, (e) and (f) for aerosol forcing, (g) and (h) for internal variability. (a), (c), (e), and (g): 1850–1967. (b), (d), (f), and (h): 1968–2014. The dots indicate that the trends pass the significance *t*-test at the 0.10 level.

mean and seasonal mean NSWSs increased were caused by the increase in the number of strong windy days from 1850 to 1967, and which decreased were caused by the decreases in the numbers of moderate and strong windy days from 1968 to 2014.

- (b) The increase in historical NSWS from 1850 to 1967 was due mainly to internal variability, which was found in nine of the ten DAMIP models, and no other forcing gave rise to pronounced NSWS strengthening from 1850 to 1967. From 1968 to 2014, the decrease in historical NSWS

was due mainly to natural, aerosol, and GHG forcings. The NSWS would decrease more significantly from 1968 to 2014 if the effects of internal variability were excluded. The NSWS PDFs with aerosol, natural, and GHG forcings were higher and narrower than the historical NSWS PDF.

In this study, the results show that the aerosols could decrease NSWS. Some studies have proposed that aerosols can induce the NSWS changes. On a continental scale, aerosols reduce surface insolation

and weaken the land–ocean thermal contrast, these inhibiting the development of monsoons. Locally, aerosol radiative effects alter the thermodynamic stability and convective potential of the lower atmosphere leading to reduced temperatures and increased atmospheric stability (Li *et al* 2016). An increase in air stability due to interactions between aerosols and radiation can reduce vertical mixing, which in turn declines the vertical flux of horizontal momentum. Since winds are generally higher aloft than at the surface, weakened vertical mixing reduces the transfer of fast winds aloft to the surface, slowing surface winds compared with those aloft and atmospheric circulations (Jacobson and Kaufman 2006). Therefore, the effects of aerosols on NSWS could be attributed to the impacts of aerosols on monsoon circulations and thermodynamic stability. The Asian monsoon region is a primary source of emissions of diverse species of aerosols; therefore, the NSWS reduction under the aerosol forcing is stronger in East Asia and South Asia than that in other regions. However, the physical mechanisms of aerosols affect NSWS and monsoons are complex, and which should be investigated systematically in future. The GHG forcing could affect the global NSWS changes through modulating the meridional atmospheric circulation (Deng *et al* 2021).

Several theories have tried to identify potential mechanisms describing how internal variability influence wind speed (Wang 2002, Timmermann *et al* 2018, Zhang *et al* 2018). For instance, the positive phase of TNA is linked with a weakened Hadley circulation and leads to a southward component of surface wind and a reduction of wind speed in the mid-latitudes (Zeng *et al* 2019). The temperature gradients during the negative and positive phases of PDO generate the easterly and westerly components of NSWS, which decrease and increase the prevailing westerly winds in the mid-latitudes, respectively (Zhang *et al* 2018). The negative and positive phases of NAO have different jet stream configurations and wind systems over Europe. Strong and weak East Asia summer monsoon are associated with increases and decreases in the surface air temperature difference between land and sea, respectively, and then which could cause the changes in NSWS (Huang *et al* 2018). Therefore, the NSWS changes over the monsoon regions could be influenced by the monsoon circulations (Xu *et al* 2006). However, the interaction and modulation among different internal variabilities are pronounced; therefore, the NSWS changes could not be simply linked with just one internal variability but should be determined by the combined effects of variations in multiple internal variabilities (Zeng *et al* 2019). In this study, we just detect that the internal variability could influence the NSWS; however, we cannot guarantee that all internal variability signals satisfy a linear relationship due to the different internal variability signals could

not be independent. The mechanism and contributions of internal variability affects NSWS should be performed in the future.

The decreases of NSWS since the 1960s in CMIP6 and the four global reanalysis products are weaker than those actually observed. Previous studies have discussed possible causes of this difference. Including, the decrease in observed NSWS is a manifestation of changes in surface roughness that are not included in the surface boundary conditions used in the climate models (Chen *et al* 2012), the current models have only a relatively weak capacity for representing some aspects of atmospheric flow (Zeng *et al* 2019), the observed trends are partly the product of non-climate-related factors, such as inhomogeneities in station settings or instrumentation (Zha *et al* 2021a), the data assimilation systems of reanalyses could contain inappropriate model topography and inaccuracies in the atmospheric boundary layer processes (Fan *et al* 2021), and the spatial resolution of the model is too coarse (Shen *et al* 2021).

The results of the present study offer new insights or at least a perspective on the changes of global terrestrial NSWS, and which could provide a scientific basis for the projections of wind speed and wind energy. However, some limitations must be mentioned. We determined potential factors inducing centennial-scale changes in NSWS, but we did not quantify their contributions and reveal the physical mechanisms of different forcings affect the centennial-scale variability in NSWS. These aspects could be carried out based on the large ensembles with different Earth system models (ESMs) due to the comparisons with large ensembles of different ESMs can reduce the uncertainty of results. Additionally, the different forcings influencing the NSWS show regional differences, and the predominant forcing factors causing regional NSWS should be quantified based on dynamical downscaling in the future.

Data availability statement

The data that support the findings of this study are openly available at the following URL/DOI: <https://esgf-node.llnl.gov/projects/cmip6/>.

Acknowledgments

We cordially thank the reviewers for their thorough comments and constructive suggestions, which improve this study significantly. We also thank all the dataset providers. The work is supported by National Key Research and Development Program of China (2018YFA0606004), National Natural Science Foundation of China (42005023, 41775087, 41875178), Project funded by China Postdoctoral Science Foundation (2019M660761), and Nanjing Meteorological Bureau Scientific Project (NJ202103). This work is also supported by the Special Research

Assistant Project of Chinese Academy of Sciences, the Program for Key laboratory in University of Yunnan Province, and the Chinese Jiangsu Collaborative Innovation Center for Climate Change.

Conflict of interest

The authors declare no competing interests.

ORCID iDs

- Cheng Shen  <https://orcid.org/0000-0003-1727-2638>
Jinlin Zha  <https://orcid.org/0000-0001-8292-7464>
Deming Zhao  <https://orcid.org/0000-0003-0063-9376>
Wenxuan Fan  <https://orcid.org/0000-0003-2457-5821>
Zhibo Li  <https://orcid.org/0000-0001-9135-1583>

References

- Alizadeh-Chobari O, Zawar-Reza P and Sturman A 2014 The 'wind of 120 days' and dust storm activity over the Sistan Basin *Atmos. Res.* **143** 328–41
Azorin-Molina C, Guijarro J A, McVicar T R, Vicente-Serrano S M, Chen D L, Jerez S and Espirito-Santo F 2016 Trends of daily peak wind gusts in Spain and Portugal, 1961–2014 *J. Geophys. Res.* **121** 1059–78
Azorin-Molina C, Vicente-Serrano S M, McVicar T R, Jerez S, Sanchez-Lorenzo A, Lopez-Moreno J L, Revuelto J, Trigo R M, Lopez-Bustins J A and Espirito-Santo F 2014 Homogenization and assessment of observed near-surface wind speed trends over Spain and Portugal, 1961–2011 *J. Clim.* **27** 2692–3712
Bichet A, Wild M, Folini D and Schar C 2012 Causes for decadal variations of wind speed over land: sensitivity studies with a global climate model *Geophys. Res. Lett.* **39** L11701
Brazdil R, Chroma K, Dobrovolny P and Tolasz R 2009 Climate fluctuations in the Czech Republic during the period 1961–2005 *Int. J. Climatol.* **29** 223–42
Chen L, Pryor S C and Li D L 2012 Assessing the performance of Intergovernmental Panel on Climate Change AR5 climate models in simulating and projecting wind speeds over China *J. Geophys. Res.* **117** D24102
Compo G P et al 2011 The twentieth century reanalysis project *Q. J. R. Meteorol. Soc.* **137** 1–28
Dadaser-Celik F and Cengiz E 2014 Wind speed trends over Turkey from 1975–2006 *Int. J. Climatol.* **34** 1913–27
Deng K, Azorin-Molina C, Minola L, Zhang G and Chen D 2021 Global near-surface wind speed changes over the last decades revealed by reanalyses and CMIP6 model simulations *J. Clim.* **34** 2219–34
Earl N, Dorling S, Hewston R and von Glasow R 2013 1980–2010 variability in U.K. surface wind climate *J. Clim.* **26** 1172–91
Eyring V et al 2019 Taking climate model evaluation to the next level *Nat. Clim. Change* **9** 102–10
Eyring V, Bony S, Meehl G A, Senior C A, Stevens B, Stouffer R J and Taylor K E 2016 Overview of the Coupled Model Intercomparison Project Phase 6 (CMIP6) experimental design and organization *Geosci. Model Dev.* **9** 1937–58
Fan W, Liu Y, Chappell A, Dong L, Xu R, Ekstrom M, Fu T M and Zeng Z 2021 Evaluation of global reanalysis land surface wind speed trends to support wind energy development using *in situ* observation *J. Appl. Meteorol. Climatol.* **60** 33–50
Fu G, Yu J, Zhang Y, Hu S, Quyang R and Liu W 2011 Temporal variation of wind speed in China for 1961–2007 *Theor. Appl. Climatol.* **104** 313–24
Fyllas N M et al 2009 Basin-wide variations in foliar properties of Amazonian forest: phylogeny, soils and climate *Biogeosciences* **6** 2677–708
Gillett N P, Shiogama H, Funke B, Hegerl G, Knutti R, Mathes K, Santer B D, Stone D and Tebaldi C 2016 The detection and attribution model intercomparison project (DAMIP v1.0) contribution to CMIP6 *Geosci. Model Dev.* **9** 3685–97
Gilliland J M and Keim B D 2018 Surface wind speed: trend and climatology of Brazil from 1980–2014 *Int. J. Climatol.* **38** 1060–73
Grose M R et al 2020 Insights from CMIP6 for Australia's future climate *Earth's Future* **8** e2019EF001469
Guan Q, Sun X, Yang J, Pan B, Zhao S and Wang L 2017 Dust storms in northern China: long-term spatiotemporal characteristics and climate controls *J. Clim.* **30** 6683–700
Guo H, Xu M and Hu Q 2011 Changes in near-surface wind speed in China: 1969–2005 *Int. J. Climatol.* **31** 349–59
He Y P, Monahan A H, Jones C G, Dai A, Biner S, Caya D and Winger K 2010 Probability distributions of land surface wind speeds over North America *J. Geophys. Res.* **115** D04103
Hersbach H, Peubey C, Simmons A, Berrisford P, Poli P and Dee D 2015 ERA-20CM: a twentieth-century atmospheric model ensemble *Q. J. R. Meteorol. Soc.* **141** 2350–75
Huang Y, Wang B, Li X and Wang H 2018 Changes in the influence of the western Pacific subtropical high on Asian summer monsoon rainfall in the late 1900s *Clim. Dyn.* **51** 443–55
Jacobson M Z and Kaufman Y J 2006 Wind reduction by aerosol particles *Geophys. Res. Lett.* **33** L24814
Jekel C F and Venter G 2019 pwlf: a python library for fitting 1D continuous piecewise linear functions (<https://doi.org/10.13140/RG.2.2.28530.56007>)
Jian B, Li J, Zhao Y, He Y, Wang J and Huang J 2020 Evaluation of the CMIP6 planetary albedo climatology using satellite observations *Clim. Dyn.* **54** 5145–61
Jiang Y, Luo Y, Zhao Z, Shi Y, Xu Y and Zhu J 2010 Projections of wind changes for 21st century in China by three regional climate models *Chin. Geog. Sci.* **20** 226–35
Karnauskas K B, Lundquist J K and Zhang L 2018 Southward shift of the global wind energy resource under high carbon dioxide emissions *Nature Geosci.* **11** 38–43
Kim J C and Paik K 2015 Recent recovery of surface wind speed after decadal decrease: a focus on South Korea *Clim. Dyn.* **45** 1699–712
Kumar D, Mishra V and Ganguly A R 2015 Evaluating wind extremes in CMIP5 climate models *Clim. Dyn.* **45** 441–53
Li Y P, Chen Y N, Li Z and Fang G H 2018 Recent recovery of surface wind speed in northwest China *Int. J. Climatol.* **38** 4445–58
Li Z Q et al 2016 Aerosol and monsoon climate interactions over Asia *Rev. Geophys.* **54** 866–929
Lin C G, Yang K, Qin J and Hu Y 2013 Observation coherent trends of surface and upper-air wind speed over China since 1960 *J. Clim.* **26** 2891–903
Liu X, Zhang X J, Tang Q and Zhang X Z 2014 Effect of surface wind speed decline on modeled hydrological conditions in China *Hydrol. Earth Syst. Sci.* **18** 2803–13
Lu R, Hong X W and Li X Y 2016 Association of rainfall and atmospheric circulation over East Asia with anomalous rainfall in the tropical western north Pacific in summer *Atmos. Oceanic Sci. Lett.* **9** 185–90
McVicar T R et al 2012 Global review and synthesis of trends in observed terrestrial near-surface wind speeds: implications for evaporation *J. Hydrol.* **24** 182–205
McVicar T R, van Niel T G, Roderick M L, Li L T, Mo X G, Zimmermann N E and Schmaltz D R 2010 Observational evidence from two mountainous regions that near-surface wind speeds are declining more rapidly at higher elevations

- than lower elevations: 1960–2006 *Geophys. Res. Lett.* **37** 1–6
- Ni Y, Zhou L, Liu Y, Wu A, Wang G, Yang X and Zhang X 1995 Study for ENSO and its influences on Asian monsoon and climate change of China *Sci. Meteorol. Sin.* **4** 30–45 in Chinese
- Pardin K M et al 2020 GCMeval—an interactive tool for evaluation and selection of climate model ensembles *Clim. Serv.* **18** 100167
- Poli P et al 2013 The data assimilation system and initial performance evaluation of the ECMWF pilot reanalysis of the 20th century assimilating surface observations only (ERA-20C) *ERA Report Series 14* (Reading: ECMWF)
- Pryor S C, Barthelmie R J, Bukovsky M S, Leung R and Sakaguchi K 2020 Climate change impacts on wind power generation *Nat. Rev. Earth Environ.* **1** 627–43
- Ramon J, Lledo L, Torralba V, Soret A and Doblas-Reyes F J 2019 What global reanalysis best represents near-surface winds? *Q. J. R. Meteorol. Soc.* **145** 3236–51
- Roderick M L, Rotstayn L D, Farquhar G D and Hobbins M T 2007 On the attribution of changing pan evaporation *Geophys. Res. Lett.* **34** L17403
- Segovia S, Gomez J D, Gallardo P, Lozano F J and Asensio C 2017 Soil nutrients losses by wind erosion in a citrus crop at southeast Spain *Eurasian Soil Sci.* **50** 756–63
- Shen C, Zha J L, Wu J and Zhao D M 2021 Centennial-scale variability of terrestrial near-surface wind speed over China from reanalysis *J. Clim.* **34** 5829–46
- Sherman P, Chen X and McElroy M B 2017 Wind-generated electricity in China: decreasing potential, interannual variability and association with changing climate *Sci. Rep.* **7** 16294
- Sherman P, Song S, Chen X and McElroy M 2021 Projected changes in wind power potential over China and India in high resolution climate models *Environ. Res. Lett.* **16** 034057
- Slivinski L C et al 2019 Towards a more reliable historical reanalysis: improvements for version 3 of the twentieth century reanalysis system *Q. J. R. Meteorol. Soc.* **145** 2876–908
- Storn R and Price K 1997 Differential evolution—a simple and efficient heuristic for global optimization over continuous spaces *J. Global Optim.* **11** 341–59
- Sun T, Che H, Wu J, Wang H, Wang Y and Zhang X 2018 The variation in visibility and its relationship with surface wind speed in China from 1960 to 2009 *Theor. Appl. Climatol.* **131** 335–47
- Timmermann A et al 2018 El Niño–Southern Oscillation complexity *Nature* **559** 535–45
- Torralba V, Doblas-Reyes F J and Gonzalez-Reyriego N 2017 Uncertainty in recent near-surface wind speed trends: a global reanalysis intercomparison *Environ. Res. Lett.* **12** 114019
- Vautard R J, Cattiaux J, Yiou P, Thepaut J N and Ciais P 2010 Northern Hemisphere atmospheric stilling partly attributed to an increase in surface roughness *Nat. Geosci.* **3** 756–61
- Wang C Z 2002 Atlantic climate variability and its associated atmospheric circulation cells *J. Clim.* **15** 1516–36
- Wohland J, Omrani N E, Withaut D and Keenlyside N S 2019 Inconsistent wind speed trends in current twentieth century reanalysis *J. Geophys. Res.* **124** 1931–40
- Wu J, Shi Y and Xu Y 2020 Evaluation and projection of surface wind speed over China based on CMIP6 GCM *J. Geophys. Res.* **125** e2020JD033611
- Wu J, Zha J and Zhao D 2016 Estimating the impact of the changes in land use and cover on the surface wind speed over the east China plain during the period 1980–2011 *Clim. Dyn.* **46** 847–63
- Wu J, Zha J and Zhao D 2017 Evaluating the effects of land use and cover change on the decrease of surface wind speed over China in recent 30 years using a statistical downscaling method *Clim. Dyn.* **48** 131–49
- Wu J, Zha J, Zhao D and Yang Q 2018a Changes in terrestrial near-surface wind speed and their possible causes: an overview *Clim. Dyn.* **51** 2039–78
- Wu J, Zha J, Zhao D and Yang Q 2018b Changes of wind speed at different heights over eastern China during 1980–2011 *Int. J. Climatol.* **38** 4476–95
- Wu J, Zha J, Zhao D and Yang Q 2018c Effects of surface friction and turbulent mixing on long-term changes in the near-surface wind speed over the eastern China plain from 1981 to 2010 *Clim. Dyn.* **51** 2285–99
- Xu M, Chang C P, Fu C, Qi Y, Robock A, Robinson D and Zhang H M 2006 Steady decline of east Asian monsoon winds, 1969–2000: evidence from direct ground measurements of wind speed *J. Geophys. Res.* **111** D24
- Yang X M, Li Z X, Feng Q, He Y Q, An W L, Zhang W, Cao W H, Yu T F, Wang Y M and Wilfred H T 2012 The decreasing wind speed in southwestern China during 1969–2009, and possible causes *Quat. Int.* **263** 71–84
- You Q L, Kang S C, Flugel W A, Pepin N, Yan Y P and Huang J 2010 Decreasing wind speed and weakening latitudinal surface pressure gradients in the Tibetan Plateau *Clim. Res.* **42** 57–64
- Zeng Z et al 2019 A reversal in global terrestrial stilling and its implications for wind energy production *Nat. Clim. Change* **9** 979–85
- Zha J, Shen C, Zhao D, Wu J and Fan W 2021b Slowdown and reversal of terrestrial near-surface wind speed and its future changes over eastern China *Environ. Res. Lett.* **16** 034028
- Zha J, Wu J and Zhao D 2016 Changes of probabilities in different wind grades induced by land use and cover change in eastern China plain during 1980–2011 *Atmos. Sci. Lett.* **17** 264–9
- Zha J, Wu J and Zhao D 2017 Effects of land use and cover change on the near-surface wind speed over China in the last 30 years *Prog. Phys. Geogr.* **41** 46–6
- Zha J, Wu J, Zhao D and Fan W 2020 Future projections of the near-surface wind speed over eastern China based on CMIP5 datasets *Clim. Dyn.* **54** 2361–85
- Zha J, Zhao D, Wu J and Shen C 2021a Research progress and prospects of terrestrial near-surface wind speed variations in China *J. Meteorol. Res.* **35** 1–21
- Zha J, Zhao D, Wu J and Zhang P 2019 Numerical simulation of the effects of land use and cover change on the near-surface wind speed over eastern China *Clim. Dyn.* **53** 1783–803
- Zhang G F, Azorin-Molina C, Chen D L, Guijarro J A, Kong F, Minola L, McVicar T R, Son S W and Shi P J 2020b Variability of daily maximum wind speed across China, 1975–2016: an examination of likely causes *J. Clim.* **33** 2793–816
- Zhang G F, Azorin-Molina C, Shi P J, Lin D, Guijarro J A, Kong F and Chen D 2019a Impact of near-surface wind speed variability on wind erosion in the eastern agro-pastoral transitional zone of northern China, 1982–2016 *Agric. For. Meteorol.* **271** 102–15
- Zhang Y, Gao L, Cao L, Yan Z and Wu Y 2020a Decreasing atmospheric visibility associated with weakening winds from 1980–2017 over China *Atmos. Environ.* **224** 117314
- Zhang Y, Xie S P, Kosaka Y and Yang J C 2018 Pacific decadal oscillation: tropical Pacific forcing versus internal variability *J. Clim.* **31** 8265–79
- Zhang Z T and Wang K C 2020 Stilling and recovery of the surface wind speed based on observation, reanalysis, and geostrophic wind theory over China from 1960 to 2017 *J. Clim.* **33** 2989–4008
- Zhang Z T, Wang K C, Chen D, Li J and Dickinson R 2019b Increase in surface friction dominates the observed surface wind speed decline during 1973–2014 in the northern Hemisphere lands *J. Clim.* **32** 7421–35